J. Mar. Sci. Eng. **2015**, *3*, 1093-1116; doi:10.3390/jmse3031093

OPEN ACCESS

Journal of
Marine Science and Engineering
ISSN 2077-1312
www.mdpi.com/journal/jmse

Article

A Flood Risk Assessment of the LaHave River Watershed, Canada Using GIS Techniques and an Unstructured Grid Combined River-Coastal Hydrodynamic Model

Kevin McGuigan, Tim Webster * and Kate Collins

Applied Geomatics Research Group, Nova Scotia Community College, Middleton, NS B0S 1M0, Canada; E-Mails: kevin.mcguigan@nscc.ca (K.M.G.); kate.collins@nscc.ca (K.C.)

* Author to whom correspondence should be addressed; E-Mail: timothy.webster@nscc.ca; Tel.: +1-902-825-2775; Fax: +1-902-825-5479.

Academic Editor: Rick Luettich

Received: 29 June 2015 / Accepted: 15 September 2015 / Published: 22 September 2015

Abstract: A flexible mesh hydrodynamic model was developed to simulate flooding of the LaHave River watershed in Nova Scotia, Canada, from the combined effects of fluvial discharge and ocean tide and surge conditions. The analysis incorporated high-resolution lidar elevation data, bathymetric river and coastal chart data, and river cross-section information. These data were merged to generate a seamless digital elevation model which was used, along with river discharge and tidal elevation data, to run a two-dimensional hydrodynamic model to produce flood risk predictions for the watershed. Fine resolution topography data were integrated seamlessly with coarse resolution bathymetry using a series of GIS tools. Model simulations were carried out using DHI Mike 21 Flexible Mesh under a variety of combinations of discharge events and storm surge levels. Discharge events were simulated for events that represent a typical annual maximum runoff and extreme events, while tide and storm surge events were simulated by using the predicted tidal time series and adding 2 and 3 m storm surge events to the ocean level seaward of the mouth of the river. Model output was examined and the maximum water level for the duration of each simulation was extracted and merged into one file that was used in a GIS to map the maximum flood extent and water depth. Upstream areas were most vulnerable to fluvial discharge events, the lower estuary was most vulnerable to the effect of storm surge and sea-level rise, and the Town of Bridgewater was influenced by the combined effects of

discharge and storm surge. To facilitate the use of the results for planning officials, GIS flood risk layers were intersected with critical infrastructure, identifying the roads, buildings, and municipal sewage infrastructure at risk under each flood scenario. Roads were converted to points at 10 m spacing for inundated areas and appended with the flood depth calculated from the maximum water level subtracted from the lidar digital elevation model.

Keywords: storm surge; flood risk mapping; sea level rise; flexible mesh; GIS

1. Introduction

The LaHave River is an estuarine river in southern Nova Scotia that has a history of both fluvial and coastal flooding. Heavy rain and snowmelt can cause the river to overflow its banks, flooding the rural communities and roads within the watershed, while storm surge and sea-level rise can cause flooding near the coast; when a heavy rainfall event is combined with a storm surge, infrastructure within the watershed is especially at risk.

This project builds on a previous study which focused on the town of Bridgewater, Nova Scotia, which is located within the LaHave River watershed [1]. In this study we expand the domain to model the entire watershed, and present modifications to the modelling in order to best represent the large and complex system. Here, as in the Bridgewater study [1] we use a seamless digital elevation model (DEM) generated using high resolution lidar elevation data, bathymetric river data, and river cross-section information, along with river discharge and tidal elevation data to run a hydrodynamic model to produce flood risk predictions. The expanded study area necessitated augmenting our previous methodology of integrating the high resolution topography data with the various sources of bathymetric data. Like Merwade and Cook [2], we approached the generation of the continuous topographic-bathymetric surface using GIS techniques.

Instead of the nested-grid approaches used in the past, in this study we employ a two-dimensional flexible mesh model, a more sophisticated and more appropriate model for the complex LaHave watershed. We use the DHI Mike Flexible Mesh model which represents a two-dimensional model of the river channel and floodplain. Flexible meshes, also known as unstructured triangular grids, are composed of triangles that can be varied in size throughout the mesh allowing the user to refine the mesh density to be higher in more critical areas and lower in less sensitive regions. This has the advantage of having higher resolution results where required while reducing computational costs in areas where only a coarse resolution is required, such as in deeper bathymetries. Additionally, flexible meshes adapt easily to follow the often irregular features of coastal and riverine systems better than rectilinear grids.

Flexible mesh modeling is a widely used and desirable basis for coastal flood models [3–5] as well as river models [6–8]. Shubert *et al.* [3] use an unstructured mesh to model coastal flooding in Glasgow, Scotland using lidar terrain data; they note the benefits of the flexible mesh density in urban areas. Kliem *et al.* [4] simulated storm surge for the North Sea-Baltic Sea using the varying resolution irregular mesh 2D shallow water model MOG2D to overcome the limitations imposed by regular grids for flood modelling. Wang *et al.* [5] used the unstructured triangular finite volume model FVCOM to more accurately represent shorelines and bathymetry; the authors coupled the hydrodynamic model with

a GIS to visualize and analyze the results and found that the simulations agreed well with observations. Hagen [6] and Gama *et al.* [7] used the Deltares-Flow-Flexible Mesh model to predict flood extent and both cited improvements in their ability to represent complex river geometries over structured grids.

Another improvement over Webster *et al.* [1] is the implementation of a spatially variable surface roughness map. Many have shown the importance of, and the differences between, including resistance parameters (e.g., Manning's n or M) through satellite imagery [8,9], landcover classification data [3], and lidar-based feature height data [10,11]. The collection of bathymetric data for rivers and shallow coastal areas is still a challenge, although new technology in the form of topo-bathymetric lidar provides the potential to acquire detail in shallow areas at a similar resolution and accuracy as traditional topographic lidar. Campana *et al.* [12] used bathymetric lidar to measure the topographic change of a river in the Italian Alps compared to manual river cross-section measurements. They conclude that bathymetric lidar offers great potential to monitor river evolution and to quantify morphological diversity. Kinzel *et al.* [13] compared the United States Geological Survey's hybrid topographic/bathymetric Experimental Advanced Airborne Research LiDAR (EAARL) sensor with detailed surveys of river channels collected using wading and sonar techniques for rivers in California and Colorado. They showed that the lidar elevation of the river bed matched the traditional survey data to on average within 30 cm. They note that the water clarity must be sufficiently clear and that the albedo river bottom must be sufficiently reflective to produce laser returns to the sensor.

1.1. Study Area

The LaHave River extends ~80 km from its headwaters at the southern base of South Mountain in the Annapolis Valley of Nova Scotia to its mouth on the Atlantic Ocean (Figure 1). The river passes through several rural communities, reaches the Town of Bridgewater approximately 20 km from the Atlantic Ocean, and passes through several more small communities before meeting the coast. The LaHave River watershed drains many lakes and rivers, covers 1686 km^2, and encompasses sections of three counties and several municipalities, including the District of the Municipality of Lunenburg, for whom this study was completed. The watershed contains a mix of land use, including industrial and residential within the Town of Bridgewater, and shifting to mainly forested and agricultural in the majority of the watershed.

The LaHave watershed includes two Ecodistricts, as defined by the Nova Scotia Department of Natural Resources [14]. The LaHave Drumlins Ecodistrict is characterized by glacial till drumlins and coniferous forests, with soils that are mostly well-drained, except between the drumlins where soil is poorly drained. The LaHave River flows through the center of the Ecodistrict until it enters the South Shore Ecodistrict near the coast. The South Shore Ecodistrict is composed of a mixture of sandy beaches, lakes and streams, and coastal forests.

Tides are semi-diurnal in the Bridgewater area, with a tidal range of 2.5 m. The tidal influence extends ~20 km up the LaHave River, just to downtown Bridgewater. The river does not ice over during the winter, but ice does form upstream of the town and in the lakes and throughout the watershed.

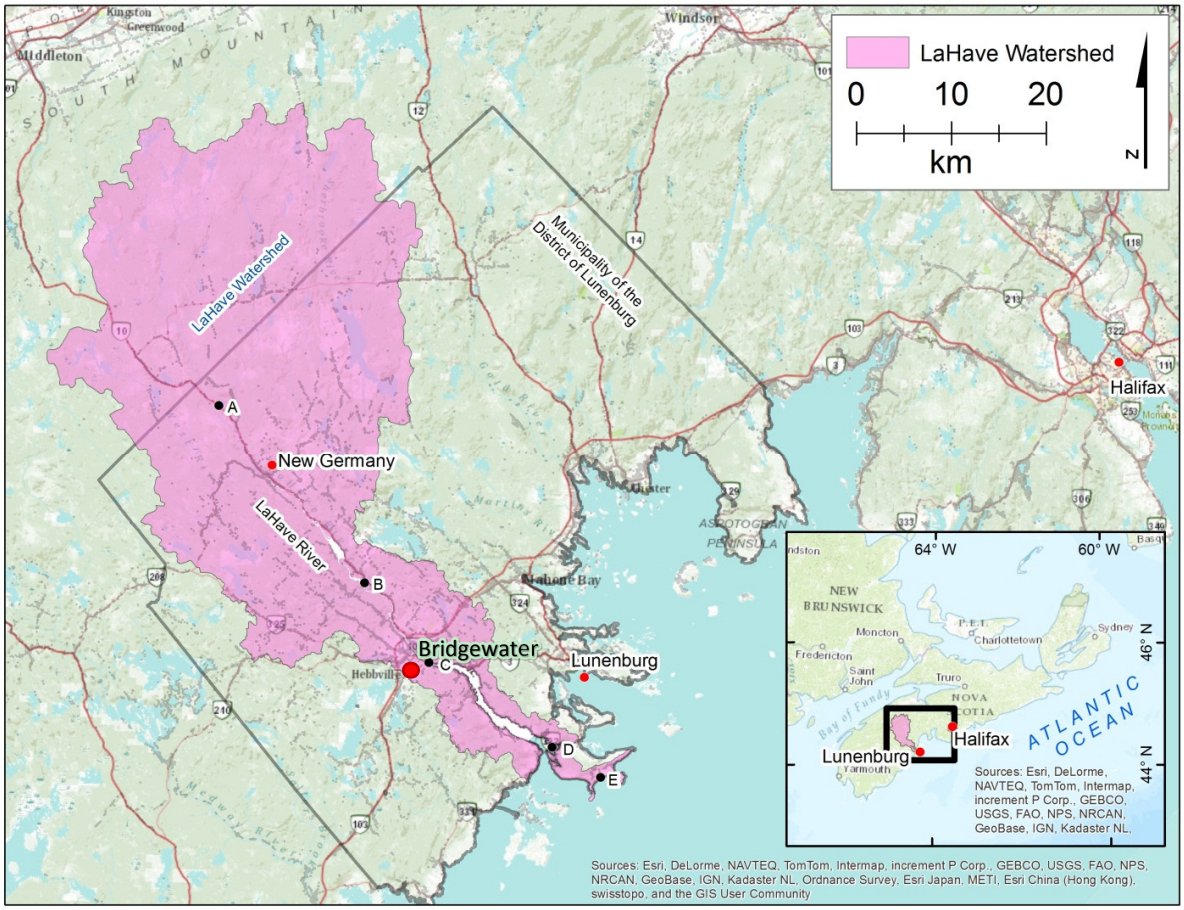

Figure 1. The LaHave River watershed extends from South Mountain, Nova Scotia, to the Atlantic Coast. (**A**) Applied Geomatics Research Group (AGRG) Cherryfield weather station; (**B**) Environment Canada water level gauge; (**C**) AGRG Marine Terminal tide gauge at Bridgewater; (**D**) AGRG Kraut Point tide gauge; (**E**) AGRG Hirtles Beach weather station.

1.2. Flood History

Storm surges can occur along the Atlantic coast when low pressure systems such as hurricanes, post-tropical storms, and Nor'easters cause high winds and heavy rain. Typically the coastal zone bears the brunt of these types of storms, but a 1 m storm surge can cause flooding and road closures 20 km inland as far as downtown Bridgewater, as occurred on 30 October No storm surge return period analysis has been completed for the LaHave Estuary directly because there is no tidal record for the area; instead, the Halifax tide gauge, located 60 km northeast along the Atlantic Coast is used for analysis (Figure 1).

Overland flooding of the LaHave River that results in property and infrastructure damage within the watershed occurs frequently and is caused by intense or prolonged rainfall, melting snow and ice, or a combination of these. Flow in the LaHave River follows a typical pattern, with maximum flow occurring in the spring and minimum flow occurring in the summer. An analysis of the 95-year LaHave River flow time series derived from the Environment Canada (EC) water level gauge in West Northfield (Figure 1) shows that almost 80% of the floods during that time period occurred during winter or spring, times when snow melt is likely to have contributed to the flood [15]. Maximum Instantaneous Peak Flow was

highest on 10 January 1956 (1080 m^3/s) and second-highest on 31 March 2003 (663 m^3/s). Both of these floods were caused by heavy rain and melting snow and caused the highest water levels ever recorded (5.73 m and 5.17 m for 1956 and 2003, respectively), 1.5 to 2.0 m higher than any other flood event in the LaHave River watershed [15]. Two fatalities occurred upstream of Bridgewater in 2003 when a car was swept off the road and into the flooded river [16].

1.3. Climate Change

In the past ten years there have been 12 Storm Surge Warnings issued by EC for Lunenburg County [17]; of these, only two events (October 2011 and February 2013 [18]) resulted in a significant storm surge and flooding. Rainfall warnings are issued far more often: eight were issued in 2013, fourteen in 2014 and six within the first three months of 2015 [17]; several of these resulted in flooding with road closures, one of which was particularly dangerous [19]. Webster *et al.* [1] showed that combined storm surge and rainfall events can produce water levels higher than would be seen with a single event, and that risk to Bridgewater is increased as sea level rises.

Much attention has been devoted on a global scale to predicting sea-level rise [20–23]. The latest assessment of the Intergovernmental Panel on Climate Change (IPCC), AR5, projects a sea-level rise for 2046–2065 of 0.17 m to 0.38 m and for 2081–2100 of 0.26 m to 0.82 m, including the effects of melting ice sheets [22]. Rahmstorf *et al.* [24] have suggested a rise between 0.5 and 1.4 m from 1990 to In Maritime Canada many coastal areas have been deemed highly susceptible to sea-level rise [25]. In Nova Scotia, global sea-level rise is compounded by crustal subsistence [26] which contributes an estimated 0.16 m per century to relative sea-level rise [27]. A comprehensive, community-by-community report prepared by Richards and Daigle [28] provides estimated extreme total sea levels for Lunenburg, a neighboring community along the South Shore of Nova Scotia located northeast of the mouth of the LaHave estuary, using Rahmstorf *et al.* [24] as a basis for sea-level rise projections. Their report presents results for 10, 25, 50 and 100-year return periods, for years 2000, 2025, 2055, 2085 and 2100, and shows that a 10-year storm could result in a sea-level of 3.29 m by 2025, 0.86 m higher than HHWLT (Higher High Water Large Tide), and a 100-year storm in 2055 would increase water level to 3.80 m.

As is the case with temperature and sea-level, precipitation and river discharge patterns are changing with climate change. In Atlantic Canada there is evidence that heavy rainfall events are increasing in frequency [29,30] an observation that agrees with models and predictions [28,29,31,32]; the increase in rainfall is expected to occur in the winter and spring [28,31]. Increased and intensified rainfall is also observed and predicted for New England [33–35]. Studies of streamflow patterns during the last 50 years show that maritime rivers in the Atlantic provinces have been experiencing lower summer flows, but higher flows in early winter and spring [36,37]. Streamflow is expected to increase with temperature and precipitation in the Atlantic region [38], and spring flooding could become more common due to changes in late-winter early-spring precipitation patterns [39].

2. Experimental Section

This project shares data and some data analysis and modelling techniques with a previous study in the same area [1]. The cases of overlap in Section 2 are identified and discussed briefly and the reader is referred to Webster *et al.* [1], while new developments are discussed in detail. The former category

includes hydrological data collection and model simulation design, while the latter category includes the GIS techniques employed to integrate topographic lidar data with coarser bathymetric data and the use of an image-derived surface roughness map. Additionally, we employ a different model, so Section 2.5 discusses the details of the flexible mesh generation, the model calibration, and boundary condition implementation.

2.1. Hydrology Data

The modelled factors driving the potential for flood risk in the LaHave Estuary include weather, river stage and tides; these data are required to run the hydrodynamic model and predict flood risk and were obtained and used in the previous Bridgewater study [1]. Discharge data for the river runoff model are from the Environment Canada flow sensor [15] (Figure 1B), additional water level data were observed near Bridgewater (Figure 1C) and near the mouth of the river (Figure 1D) using AGRG pressure sensors. Air pressure data used to compensate the water level sensors came from AGRG weather stations in the center of the watershed (Figure 1A) and the Atlantic coast (Figure 1E).

2.2. DEM Development

An accurate representation of bathymetry and topography is essential for successful hydrodynamic flood risk modelling. In this study bathymetry data from a suite of data sources were combined with topographic lidar data to generate a continuous DEM that was used in the model.

2.2.1. Bathymetric Survey

A bathymetric grid was compiled from a variety of sources to accurately represent seabed, lakebed and river channel bathymetry as well as their geometries (Figure 2). Lake bathymetry was obtained from the Nova Scotia Department of Fisheries and Aquaculture [40] (Figure 2a). Upstream of Bridgewater a combination of depths were measured using a depth sounder mounted on a canoe (Figure 2b) and for extremely shallow locations RTK GPS and depth measurements were obtained manually by walking across the river (Figure 2c), and from Bridgewater to Upper LaHave the depth sounder was mounted on a 15 foot aluminum boat. The Canadian Hydrographic Survey (CHS) nautical chart Chart 4381 at a scale of 1:38,900 was digitized to obtain soundings between Upper LaHave and Riverport (Figure 2d) and the digital chart covered the area from Riverport to the coast, including the mouth of the LaHave River. Areas where no bathymetric information existed were modelled to artificially form a channel using a method discussed in Section 2.2.3 (Figure 2e–g).

2.2.2. Lidar Survey

Lidar data for this project were obtained for the coastal region in 2009 [41] and for the remainder of the watershed in 2012 [1] at ~1 m spacing. Two surface models were constructed from these data; a Digital Surface Model (DSM) which incorporates all the points and a bare-earth DEM which incorporates only the classified ground points.

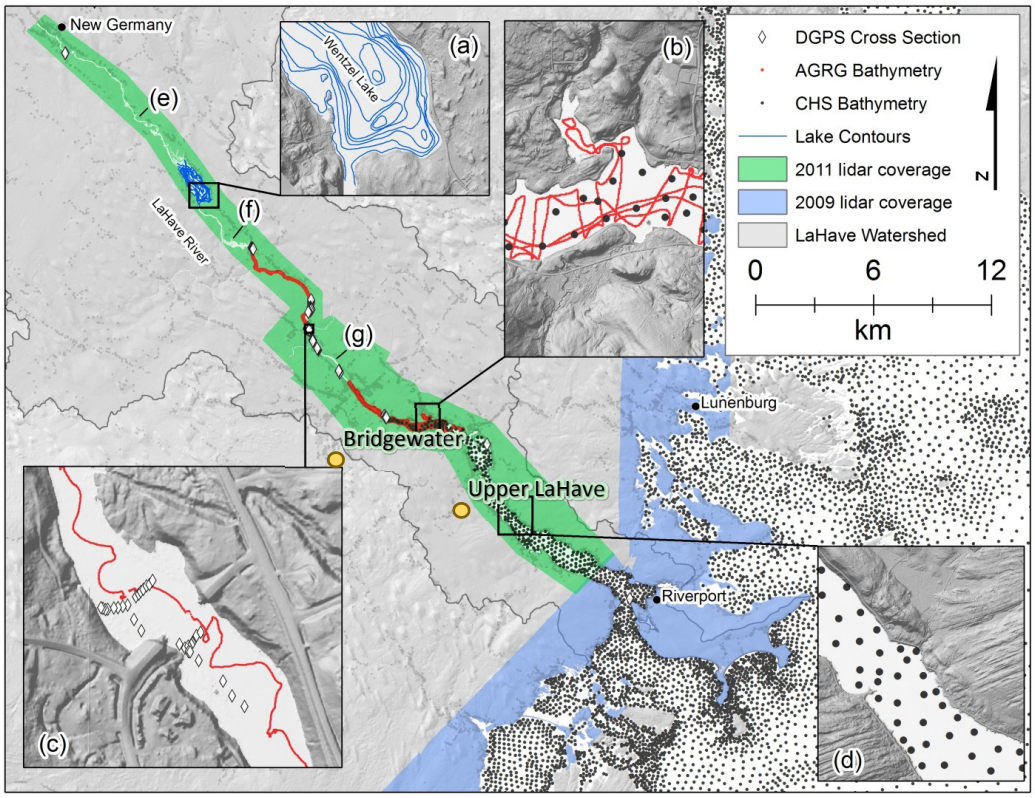

Figure 2. Topo-bathymetric data sets amalgamated in this study include (**a**) lake bathymetry contours; (**b**) AGRG bathymetry from canoe survey; (**c**) AGRG RTK GPS cross sections; (**d**) CHS bathymetry from paper chart; (**e**–**g**) areas of no bathymetric information where the channel was modified. Blue area represents the lidar coverage from 2009, green area represents the lidar coverage from 2012.

2.2.3. Topographic-Bathymetric Data Integration

The lidar survey provides sufficient detail to model the floodplain but it does not penetrate the water surface and must be combined with the bathymetry data to generate a seamless topo-bathymetric DEM that represents the topography above and below the water line. The water surface extent was delineated from the combined 2011 and 2009 lidar datasets on a 2 m spatial resolution using a custom built ArcGIS tool that is based on user input cross-sections, as described in Webster *et al.* [1]. The water surface was refined with additional cross-sections and manual digitization where necessary.

The process of integrating the bathymetry data with the lidar data differs from and improves upon the previous study [1]. Here, all bathymetric data from New Germany to Riverport (Figure 2) were averaged by depth into a 12 m grid; the digital CHS chart covering the coastal area was dealt with separately and is discussed later. The river bank was identified using the water surface extent and a 4 m landward buffer. Bathymetry points that were within a specified distance to the river bank were removed to reduce severe oscillations in subsequent bank-bathymetry interpolations. The river bank then contained only lidar points at 2 m resolution, and these were assigned a value of 0 m depth. The bank points were then integrated with the now 12 m gridded bathymetry points at 16 m resolution using a spline interpolation method, and resampled to a 4 m resolution water depth grid ("observed spline"). A buffer extending

from the river bank points to 10 m landward of the lidar bank points was used in the spline to eliminate interpolation calculations occurring between river segments.

Where bathymetry data were nonexistent (Figure 2e–g) an experimentally determined depth model was developed based on Euclidian distance from the banks in areas of known bathymetry, such that:

$$h = \frac{(x^{0.4} + 0.1x)}{3.5} \quad (1)$$

where h is water depth relative to the bottom and x is the Euclidian distance. Modelled depths were sampled to 12 m spacing and points within a 4 m distance of the river bank were removed. A spline was generated at a 4 m resolution using modelled and observed bathymetry points, lidar bank points, and a 10 m landward bank-buffered spline barrier ("modelled spline"). The resulting grid indicated that modelled depth values tended to over-estimate channel depth in some areas, specifically near the town of Bridgewater, producing an artificial scouring effect (Figure 3a). This is to be expected as the depth model was designed to predict bathymetry further upstream where channel banks are steeper and the river is shallower. To combine the modelled and observed bathymetry more smoothly, a 1 bit raster mask was used to remove modelled bathymetry points in areas where the "modelled spline" depth points were more than 0.50 m deeper than the "observed spline" depth points (Figure 3b). Furthermore, a manual estimation of water depth was included as points where some narrow sections of the LaHave water surface were unaccounted for by this technique (Figure 3c) and the spline interpolation was recomputed to generate a final river bathymetry grid (Figure 3d).

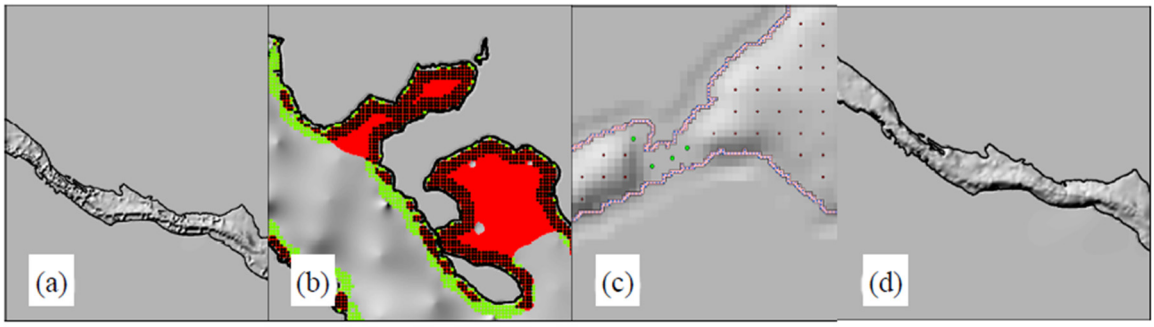

Figure 3. (**a**) The initial modelled-observed bathymetry interpolation; (**b**) the mask used to remove poorly modelled bathymetric points: red points were kept and green points discarded; (**c**) the resultant spline with no artificial scouring; (**d**) additional bathymetry was added manually as required (green points).

The river bathymetry grid was bi-linearly resampled to a 2 m spatial resolution and subtracted from the 2 m resolution lidar DEM with the water surface included (Figure 4); this generated a DEM of lidar topography and river bathymetry for the lidar extent. Sections where noise, offsets, or artifacts existed in the water surface of the lidar were selected and smoothed using a low-pass filter, or removed. The tidal portion of the study area extended ~15 km from Riverport into the Atlantic Ocean (Figure 2). This area was outside of the lidar extent and so was modelled using 20 m Nova Scotia Topographic Database (NSTDB) elevation data up to 10 m relative to the Canadian Geodetic Vertical Datum of 1928 (CGVD28) merged with the CHS digitized chart bathymetry; the resulting coastal DEM was merged with the

river DEM to generate a seamless topographic-bathymetric model of the LaHave River estuary relative to CGVD28.

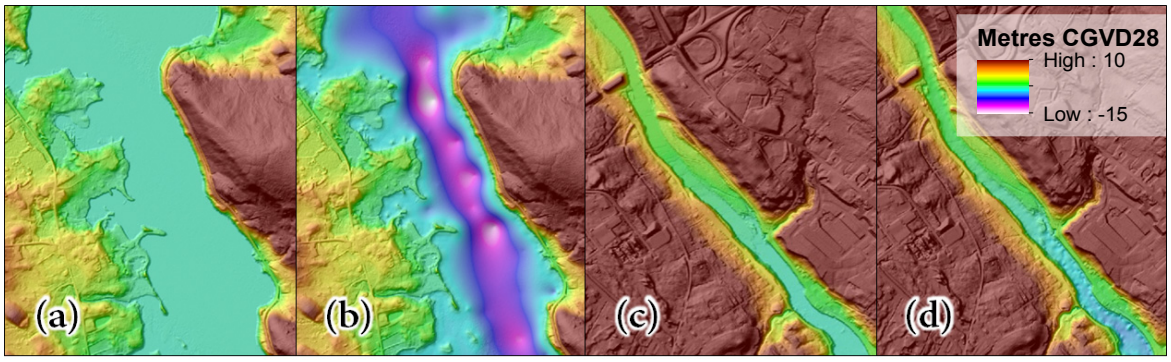

Figure 4. Lidar data before (**a**,**c**) and after (**b**,**d**) bathymetric integration; An area upstream of Bridgewater is shown in (**a**,**b**); downtown Bridgewater is shown in (**c**,**d**).

2.3. Unstructured Mesh Generation

An unstructured grid, or flexible mesh, was generated from the seamless 2 m topographic-bathymetric DEM using the Mike DHI mesh generator toolset (Figure 5). Before computation of the flexible mesh, the modelled domain was limited to areas where flooding was possible by calculating a maximum flood extent. To accomplish this, the slope of the LaHave River level was determined through the use of a flow accumulation calculation, and an approximate maximum flood level (z_{max} relative to CGVD28) along the river channel was calculated such that:

$$z_{max} = 0.89z + 10 \quad (2)$$

where z refers to vertical elevation relative to CGVDThis function was developed such that the maximum flood level would be limited to 10 m above areas with a river level of 0 m CGVD28 (which can accommodate a storm surge of approximately 8.5 m if necessary) and flood levels upstream at the head of the river (62 m CGVD28) would have a maximum flood level of ~65 m CGVD28, or a maximum flood depth of ~3 m. The maximum flood extent was generated by buffering points along the river by a factor based on the flow accumulation, calculating the maximum flood level using Equation (2), and intersecting the resultant surface with the seamless DEM. The maximum flood extent was used to generate the outer boundary of the flexible triangular mesh grid (Figure 5). The boundary was smoothed using the Polynomial Approximation with Exponential Kernel (PAEK) algorithm with a smoothing tolerance of 20 m to eliminate sharp angles of the boundary originating from the vectorization of the maximum water level raster.

The boundary was also used to clip the lidar elevation grid to reduce the input of elevation data into the Mike DHI mesh building tool. Topographic data density was reduced further using a key-point analysis to eliminate redundant elevations while preserving geometry to within 0.10 m; this technique reduces the number of points in a mesh but still provides an accurate representation of the topography. The mesh density was further customized to increase model stability and reduce simulation time by separating it into sections of varying mesh density. Mesh density near the river banks was defined to increase linearly with slope and elevation, and the remainder of the mesh was designed following the

advancing-front method [42] so that it varied in density from 50,000 m^2 maximum area per triangle element in the coastal region (Figure 5c); to 500 m^2 in the densest regions upstream (Figure 5a,b). All triangles were built with a minimum allowable angle of 26 degrees.

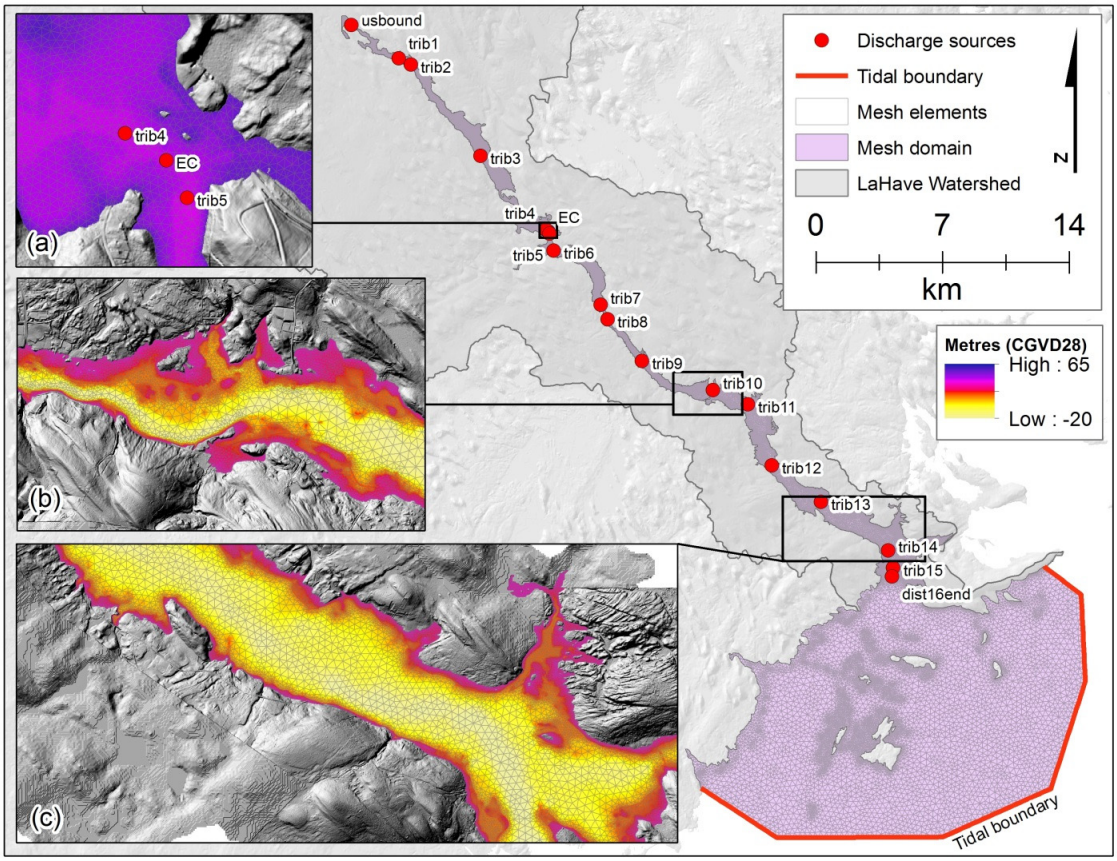

Figure 5. Flexible mesh modelling domain with tidal and discharge (tributary) boundary locations. (**a**) Inset of the mesh at the EC gauge; (**b**) variable mesh density and elevation midway along the estuary; (**c**) variable mesh density and elevation midway near the mouth of the estuary.

2.4. Surface Roughness Map

The stability and calibration of coupled coastal-fluvial hydrodynamic flood models depends in large part on the accurate representation of dynamic flow characteristics over varying surfaces such as cobbled streams, vegetation and concrete. As such, bed roughness indices were employed to model the observed relationship between depth-averaged flow velocity and total water depth across varying bed types. To represent this relationship spatially the model included a variable Manning's M index grid, for which small numbers represent the roughest surfaces and most resistance to flow, and the largest numbers represent the smoothest surfaces and least resistance to flow; Manning's M is the reciprocal of the commonly used Manning's n. Here, we used a single Band 5 (near infrared) 30 m resolution Landsat 5 image (taken 27 July 2008) to develop a 10 m resolution surface roughness grid based on vegetation density and land use (Table 1).

Table 1. Derivation of Manning's M spatial roughness grid.

Feature				Manning's M
Vegetation	Heavy	Digital Number	16–54	10
	Medium		55–69	15
	Light–none		>70	20
Initial value for river channel and coast				25
Roads				90

2.5. Hydrodynamic Modelling

There are many approaches to the hydrodynamic modelling of estuarine systems, all with various levels of detail and requirements. This model was designed using the Mike DHI software wherein a 2-d depth averaged incompressible Reynolds averaged Navier-Stokes shallow-water equation was solved over the constructed flexible mesh domain with a variable time step scheme. Operationally the simulations ran at an average time step of approximately 0.4 s. The shallow water equations used allowed for variation in temperature, salinity, and density, but all were assumed constant in this study to decrease processing time. Ideally, discharge data would be available for each tributary entering the LaHave River to incorporate river discharge from the whole watershed into the downstream tidal model (Figure 5). In the absence of these data, our approach was to include discharge from all major tributaries as discharge point sources, each scaled relative to a single long term observed discharge record which exists in the mid-section of the model domain. Catchments for the 17 tributaries were defined using a flow accumulation calculation for the entire LaHave watershed executed on a 20 m spatial resolution DEM using available NSTDB data. Each source point was assigned a scale factor based on the area of its catchment relative to the drainage area of the LaHave River EC gauge (Table 2). Additional discharge sources intermediate to defined tributaries were included in tributary point sources downstream. The scale factors were applied to the EC daily discharge record [15] resulting in a discharge time series for each tributary. This approach allowed the model to be linked to a large amount of discharge data for statistical purposes while not being required to analyze rainfall rates or the complexities of snow melt, both of which are inherent to the discharge record; additionally, we were able to incorporate contributions from all catchments without deploying sensors at each tributary location. This method is limited by the assumption that all catchments in the watershed have the same hydrological properties. The scaled discharge time series were used as boundary conditions that were varied for each model simulation and area discussed in Section 2.5.2.

Table 2. Major LaHave River tributaries, catchment contributions, and scale factor applied to the EC gauge discharge.

Name	Catchment Contribution (Number of 20 × 20 m Pixels)	EC Gauge Ratio
EC Gauge	3,113,163	1.00000
usbound	1,781,664	0.57230
trib3	1,148,538	0.38428
trib6	459,567	0.14796
dist16end	14,972	0.00481

2.5.1. Model Calibration

The model was calibrated by comparing observed water levels at the EC gauge, near the town of Bridgewater, and at the mouth of the river (locations shown on Figure 1) to modelled water levels extracted from the model at those locations. All water level recording equipment were referenced vertically to the datum of the model (CGVD28) using survey grade RTK GPS (with a precision of 2.5 cm or better). Tidal calibration was done for 8–15 August 2012 which was selected as a period where the predicted and gauged tides were most congruent and did not exhibit any high frequency variations observed during the winter (Figure 6a,b). At Kraut Point (Marine Terminal) the mean difference between modelled and observed water level was −1.5 cm (−5.2 cm), standard deviation 24 cm (15 cm). This very low mean difference between the modelled and observed water levels in the southern portion of the model domain (Kraut Point, Figure 1) indicates that the tidally dominated portion of the flow model operates very accurately, specifically during non-storm events. A discharge event on 1 November 2012 was used for the fluvial model calibration as the river water level conditions before the event were stable and the curve of the event was smooth and thus near the signature desired to be used for the various flood simulations (Figure 6c).

In the calibration phase, all hydrodynamic parameters were determined and remained consistent for all subsequent flood scenario simulations (Table 3). Principal parameters which contributed to the fluvial calibration include the relative timing of discharge sources upstream of the EC gauge as well as the bed roughness of the river. It was experimentally determined that each of the discharge sources upstream of the EC gauge (usbound, trib1, trib2, trib3) should be shifted by several hours (7, 5, 5, 2, respectively). A Manning M value of 33 was determined for the river channel and the coastal domain of the model using a trial and error process of model and observation time series comparison. A small section on the edge of the tidal boundary was assigned a very rough Manning M value of 5 to eliminate oscillations which existed along the boundary and thus improved model stability.

Table 3. Final model parameter values.

Parameter	Value
Time step	Variable, 0.01–30 s
Critical CFL number	0.8
Drying Depth	0 m
Flooding Depth	0.05 m
Wetting Depth	0.1 m
Density Type	Barotropic
Smagorinsky eddy viscosity coefficient	0.28
Final Manning M of river channel and most of coast	33
Final Manning M at tidal boundary	5

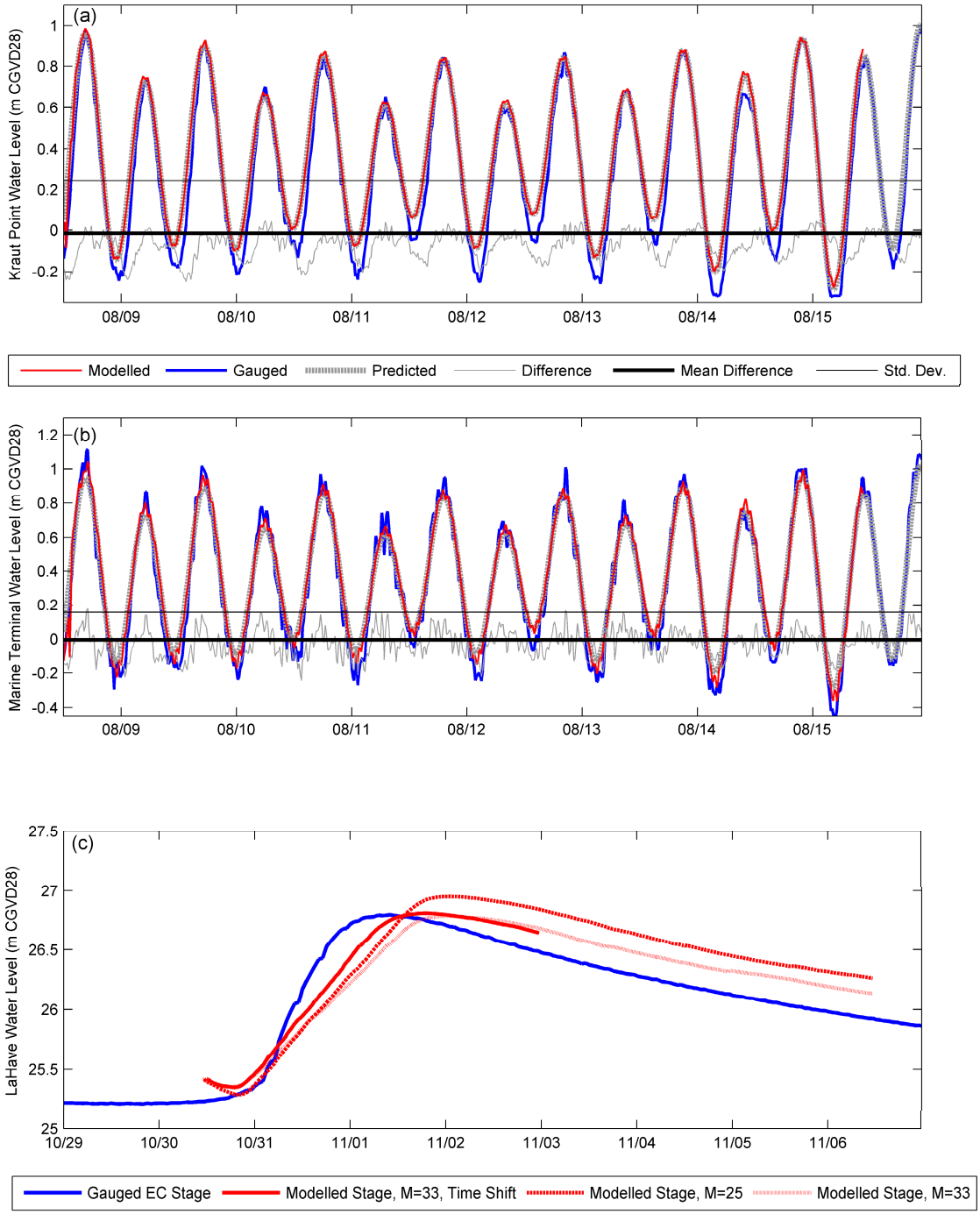

Figure 6. (**a**) Comparison of tide gauge observations with model results at Kraut Point (mean difference −1.5 cm, standard deviation 24 cm); (**b**) comparison of tide gauge observations with model results at the Marine Terminal (mean difference −5.2 cm, standard deviation 15 cm). Predicted tide used for the model boundary is plotted on both (**a**,**b**); **(c)** shows gauged and modelled stage of the LaHave River at the Environment Canada Gauge location. Three different model results are shown with variable Manning's M; the final model version (solid red line) uses M = 33 and a time shift. Note that (**a**,**b**) share the same legend; (**c**) references the legend at the bottom of the figure.

2.5.2. Model Simulations

2.5.2.1. Extreme Value Analysis

In this study we are examining the risk of flooding from two possible sources which can interact to compound the problem: river runoff and storm surges or long-term sea-level rise. The model scenarios follow Webster *et al.* [1], who use extreme value models (EVMs) to determine the return periods of extreme events using the discharge and sea-level time series to examine how often such events have occurred in the past. The time series of measured discharge of the LaHave River (1915–2012) was used to determine the annual probability of extreme events and also the return period of extreme high flow events. Table 4a summarizes the return period in years and the associated discharge for a 65% probability of occurrence, which equals at least one occurrence. Re-examining the historical high discharge events of January 1956 and March 2003, we see that the 1956 event has a recurrence interval greater than 100 years (1080 m^3/s), while the 2003 event (663 m^3/s) is approximately equivalent to a 50 year return period event with a 65% probability of occurrence.

Table 4. Model simulations. Simulation naming scheme format: first 3 digits indicate a discharge return period of 0, 50 or 100 years, last digit indicates level of storm surge (0 for maximum high tide conditions, 2 for a 2.0 m surge on top of the predicted tide or 3 for a 3.0 m surge on top of the predicted tide).

(a) LaHave River Scenario			(b) Sea Level Scenario		
Probability	**Return Period**	**Discharge (m^3/s)**	**Max. High + 0.0 m**	**Max. High + 2.0 m**	**Max. High + 3.0 m**
65%	0 year	210	Sim000_0	Sim000_2	Sim000_3
	50 year	652	Sim050_0	Sim050_2	Sim050_3
	100 year	741	Sim100_0	Sim100_2	Sim100_3

The Halifax tide gauge record (1920–2010) was used to estimate the risk or probability of flooding related to high water events along the coast [1,41]. The 100-year return period flood level under current RSL conditions is 2.2 m [1], which is 10 cm below previous high water level maximum observed during Hurricane Juan in Halifax in 2003 which had an associated storm surge of 1.63 m [27]. If RSL increases to a rate of 0.73 m/century [21], the 100 year water level increases to 2.5 m CGVD28 which further inundates areas. If RSL increases to a rate of 1.46 m/century [24], the 100 year water level increases to 3.1 m CGVDIn this study, we use these estimates as guidelines, and use storm surge levels of 0.0 m, 2.0 m and 3.0 m (Table 4b) added to the maximum predicted high tide for These values can be thought of as extreme storm surges today or moderate surges in the future considering RSL.

Three sets of model simulations were executed for each different return period discharge: one set based on variable discharge under maximum high tide conditions in 2012, and two other sets based on different storm surge or long-term sea-level rise conditions (Table 4).

2.5.2.2. Boundary Conditions

The discharge and storm surge scenarios were implemented using boundary conditions (Figure 7). The river discharge boundary condition was scaled proportionally to the drainage area for the LaHave

River as described above and varied according to the 0, 50 and 100 year return period discharge values (Figure 7a,b). We obtained predicted water level time series from the DHI Global Tidal Model, which includes the 10 major tidal constituents [43]. The storm surge scenarios (0.0 m, 2.0 m, and 3.0 m water levels) were added to the predicted maximum 2012 high tide boundary (Figure 7c) at the mouth of the LaHave River (Figure 5). The timing of the peak river discharge relative to the storm surge peak was determined experimentally, after calibrating for surface roughness, to ensure the worst case flooding condition.

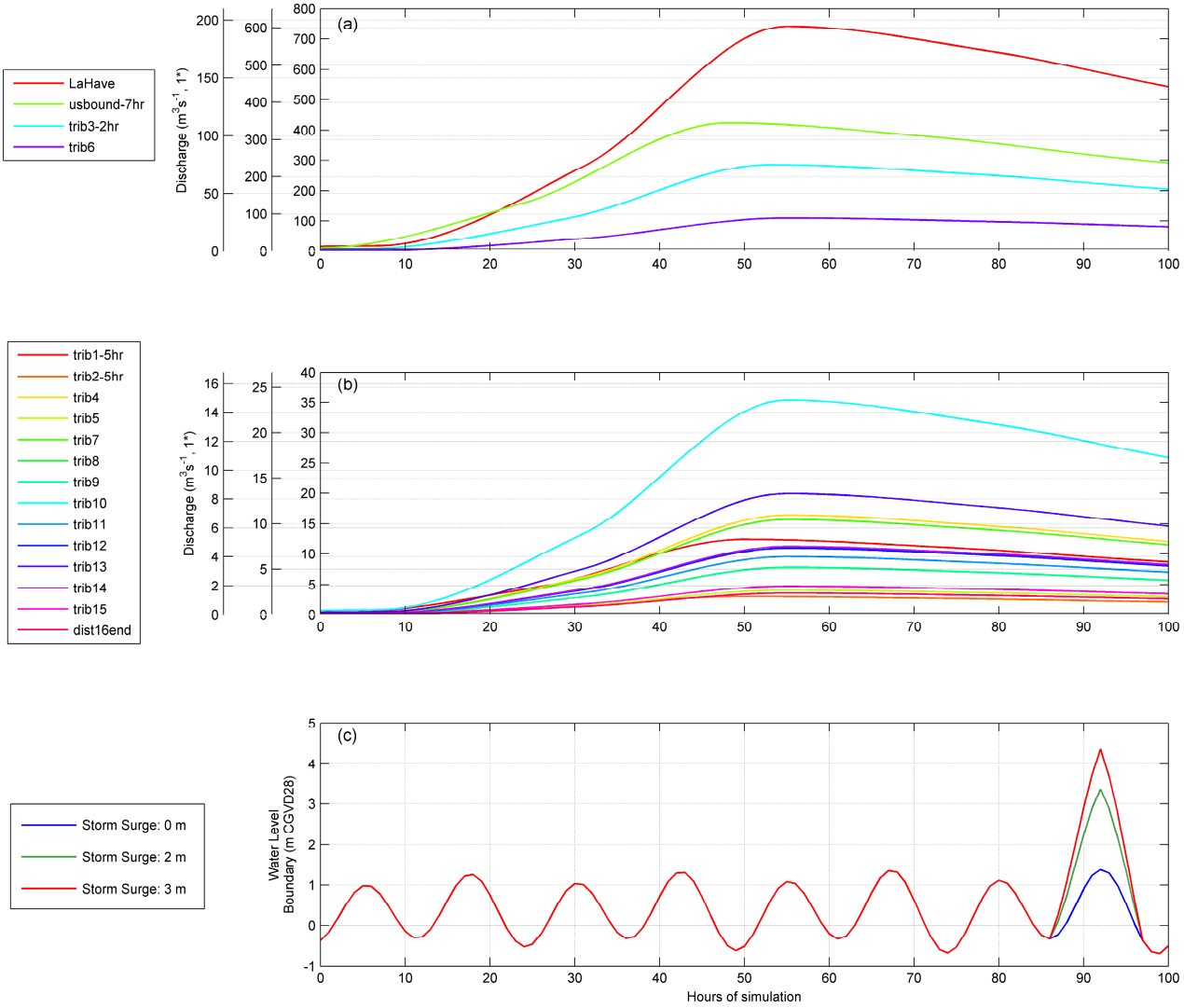

Figure 7. Model Boundary Conditions for (**a**) discharge at major tributaries for 0, 50, and 100 year return level flows; (**b**) discharge at minor tributaries for 0, 50, and 100 year return level flows; (**c**) tidal boundaries for storm surge levels 0 m, 2 m, and 3 m.

3. Results and Discussion

3.1. Simulation Results

Maximum water level from each of the nine simulations were output from Mike as flexible mesh elements and interpolated to a surface which was intersected with the DEM. The simulation naming

scheme format is as follows: the first 3 digits indicate a discharge return period of 0, 50 or 100 years, the last digit indicates level of storm surge (0 for maximum high tide conditions, 2 for a 2.0 m surge on top of the predicted high tide or 3 for a 3.0 m surge on top of the predicted high tide). Analysis of the results of all nine simulations revealed that the area upstream of Bridgewater is dominated by discharge events with limited flooding from elevated sea-level (Figure 8), the area around Bridgewater is influenced by the combined effects of discharge and sea-level (Figure 9), and downstream of Bridgewater is dominated by elevated sea-levels and less by major discharge events (Figure 10). We present results of three simulations, Sim000_0, Sim050_2, and Sim100_3, which represent the range of conditions from typical annual events to rare extreme events.

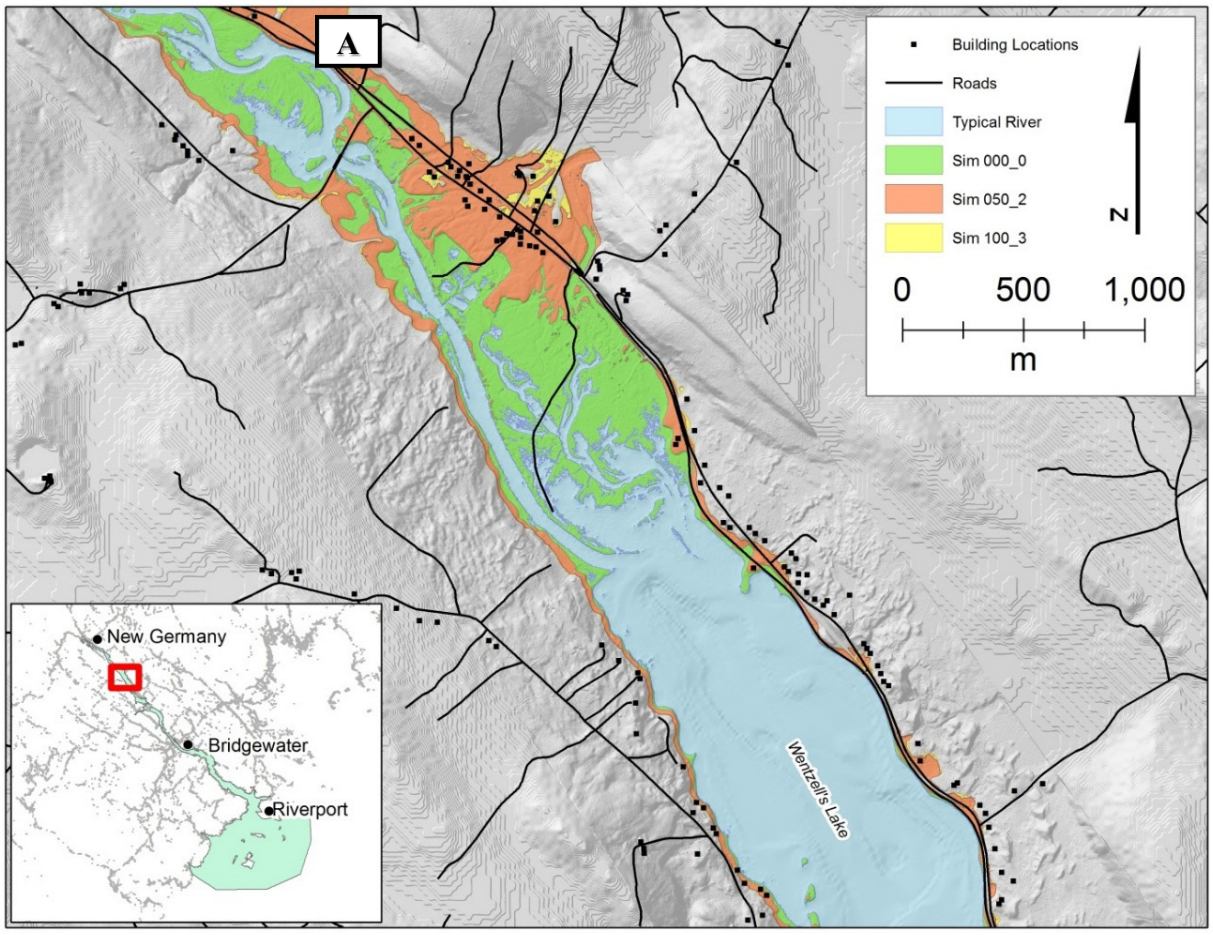

Figure 8. Maximum flood extents from Sim000_0 (green), Sim050_2 (orange) and 100_3 (yellow) south of New Germany. The normal river extent is shown in blue and the road (black lines) and buildings (black squares) effected. The background image is a combination of the lidar and 20 m DEM. "A" marks the location of two deaths in 2003 during a March flood event.

Although Sim050_2 shows flooding around New Germany (Figure 8) from the 1 in 50 year return period discharge with a 2 m storm surge on high tide in orange, a similar flood extent is observed for this area when we plot Sim050_0 which represents the 1 in 50 year return period discharge with high tide indicating there is virtually no influence of the sea-level at the mouth of the LaHave estuary for this

area. The 100 year discharge event only increases the maximum flood extent slightly (yellow Figure 8). There are significant impacts from flooding for the 50 year discharge event including overtopped road and abandoned rail lines and flooded buildings on the east side of the river. The discharge values for Sim 050_2 and the March 2003 flood event are similar, and the simulation shows flood extents that agree with observations of road overtoppings in this area, including the area where two people died because they could not see the inundated road and drove into the ditch and drowned (Figure 8A).

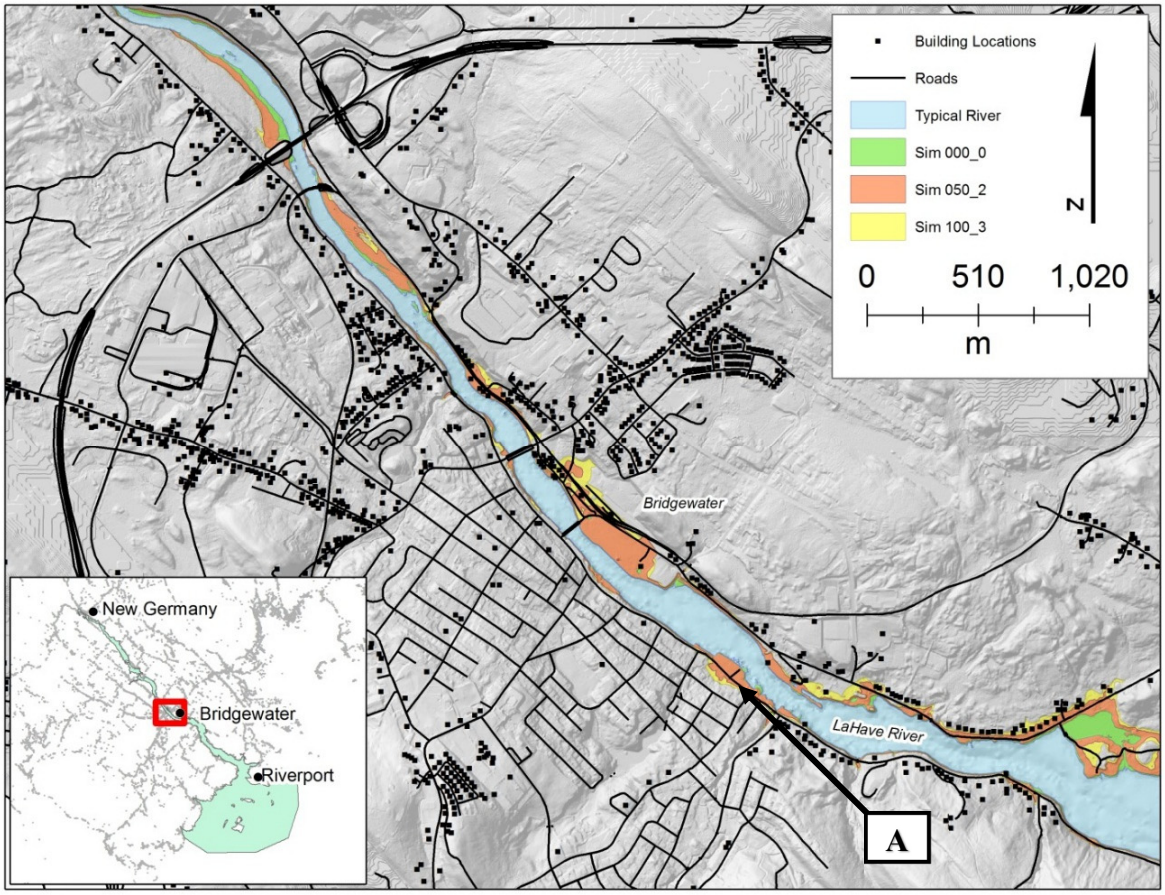

Figure 9. Maximum flood extents from Sim000_0 (green), Sim050_2 (orange) and 100_3 (yellow) at Bridgewater. The normal river extent is shown in blue and the road (black lines) and buildings (black squares) effected. The background image is a combination of the lidar and 20 m DEM. "A" shows the location of flooding during the 2 m storm surge in October 2011.

The influence of the 1 in 50 year discharge scenario dominates the flooding resulting from Sim 050_2 until immediately upstream of Bridgewater. Downstream, the effects of storm surge dominate the flooding from Sim 050_2; Figure 9 shows the Bridgewater Mall parking lot flooded due to the 2 m storm surge. Farther downstream of Bridgewater the 2 and 3 m storm surge water levels flood sections of the highway, parks, and buildings. In October 2011 a 2 m storm surge was observed to flood the Bridgewater waterfront, especially at Shipyards Landing Park (Figure 9A).

The area from Upper LaHave downstream to the mouth of the river at Riverport is vulnerable to elevated sea-level scenarios where the 2 and 3 m storm surge levels inundate and overtop the roads on

both sides of the river (Figure 10), matching photographic evidence of flooding in these locations during the October 2011 storm surge event.

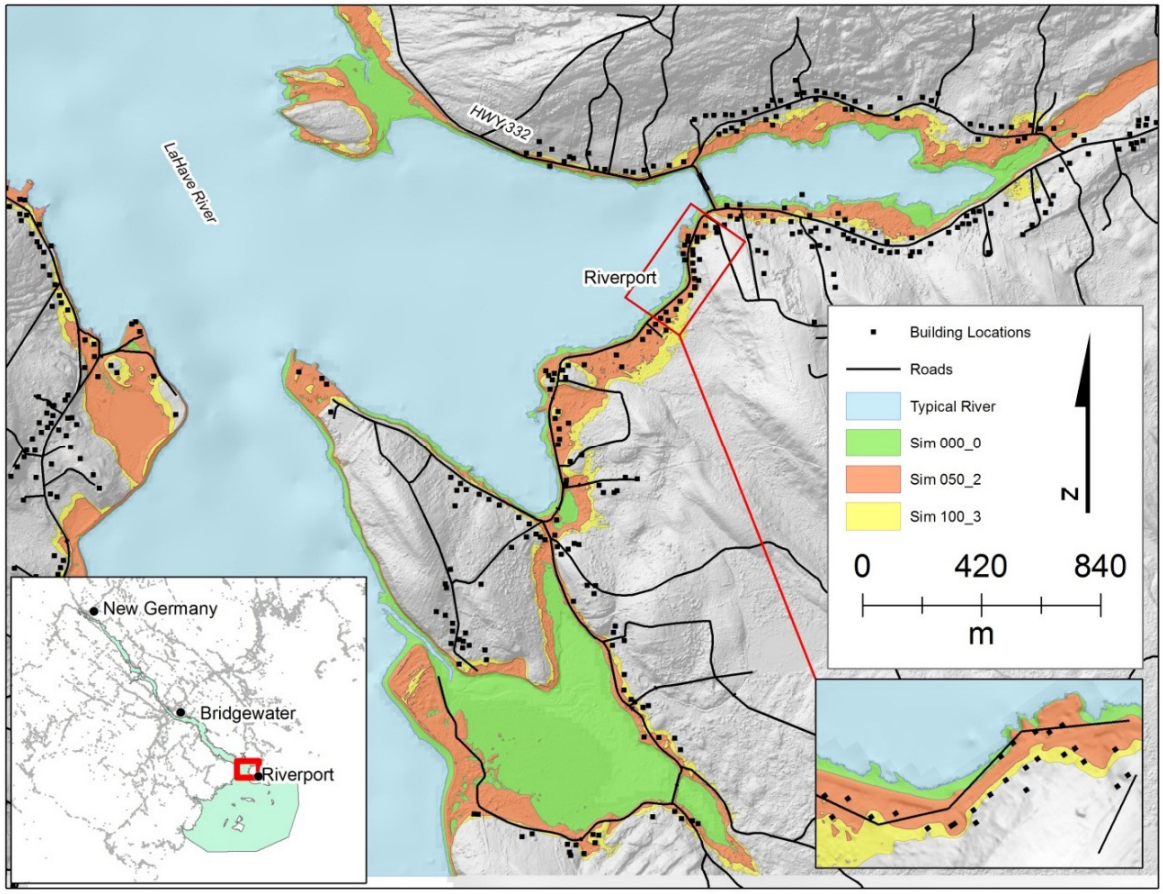

Figure 10. Maximum flood extents from Sim000_0 (green), Sim050_2 (orange) and 100_3 (yellow) at Riverport. The normal river extent is shown in blue and the road (black lines) and buildings (black squares) effected. The background image is a combination of the lidar and 20 m DEM.

3.2. Infrastructure Risk Assessment

An infrastructure risk assessment was conducted based on the nine simulations. Road vectors were segmented at 10 m intervals into points and overlaid on the flood depth maps from the model simulations along with points representing buildings, manholes and pump stations. Maximum water depths were tabulated for each flood scenario per point where flooding had occurred. The infrastructure exhibited a range of impact levels varying by location along the river and by the various flood scenarios (Figure 11). This point analysis approach enables a quick assessment of the at risk infrastructure along the river. Infrastructure in the northern portion of the model domain, which flood as the result of fluvial runoff, exhibit only minor flooding in annual maximum discharge conditions (Figure 11a,c). Roads, though sometimes bounded by flood waters on either side, are typically not overtopped in this case. Flooding becomes much more severe and infrastructure is widely affected and even overtopped upstream during a 50 year discharge event and more severely so during a 100 event. Roadways which may have been inundated yet traversable in the 50 year event can become impassable due to an increase in water depth

during a 100 year discharge event. A similar relationship can be observed in the depth over roads in the 2 m and 3 m storm surge simulations in the tidal flooding dominated southern portion of the study area (Figure 11b,d).

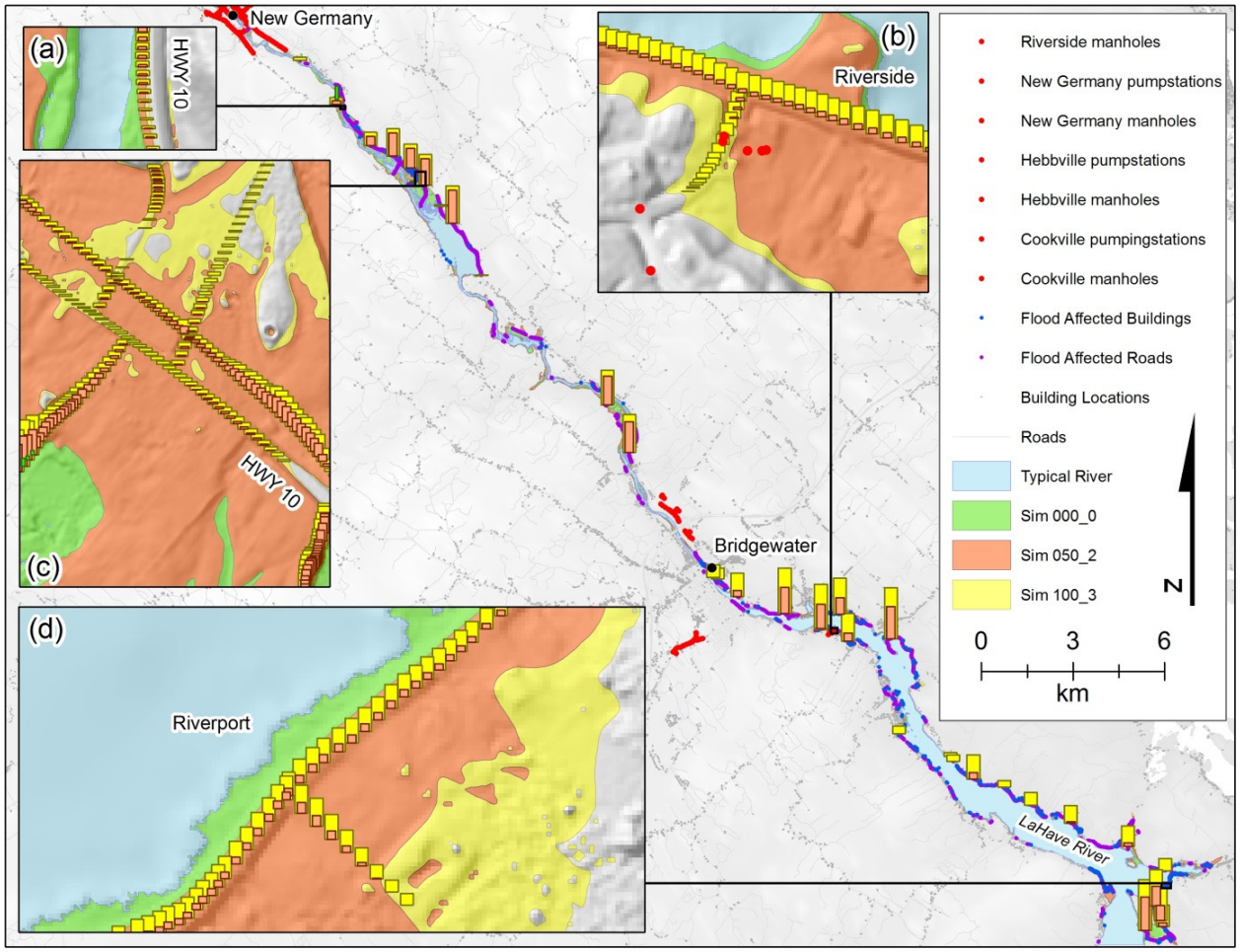

Figure 11. The infrastructure assessment of flood risk along the LaHave river study area indicates a wide range of risk from both discharge (north of Bridgewater, (**a**,**c**)) and storm surge (south of Bridgewater, (**b**,**d**)). At-risk roads (purple), buildings (blue), and sewers (red) are indicated. Relative water depths over infrastructure are indicated as bar graphs and color coded by flood simulation (Sim 000_0, Sim 050_2, and Sim 100_3).

3.3. Discussion

3.3.1. Interpretation and Implications

The results of this study agree with and improve upon the findings of Webster *et al.* [1] who studied a limited portion of the LaHave watershed to estimate flood risk only within the town of Bridgewater. Here, we do a far more in-depth examination of flood risk in the entire watershed. This required a more complex integration of high resolution lidar topography data with several additional sources of different resolution bathymetry; but most importantly, expansion of the model domain allowed us to indicate which areas were most at risk to different discharge or sea-level flood scenarios. The precise division of

areas at risk to each type of flooding provided invaluable information to municipal planners and emergency response officials as it allows them to customize their Emergency Response Operations and develop their urban planning strategies with a more directed spatial approach. Once an integrated fluvial-coastal hydrodynamic analysis is completed, at-risk infrastructure mapping can be relatively trivial and is an effective tool for the municipality to prioritize allocation of infrastructure funding.

Perhaps the most original contribution of this study is the specific approach developed to smoothly amalgamate coarse bathymetry points with the much finer resolution topographic lidar data, most notably the use of a combination of measured and predicted water depths to seamlessly fill large gaps in measured bathymetry and populate the flexible mesh.

The approach taken in this study to derive discharge contributions from along the river (tributaries) simply by way of cumulative catchment areas scaled using a single gauged location was an efficient and effective method to incorporate total watershed flow; however, it presumes that all catchment runoff characteristics throughout the watershed are identical, or perform similarly to the gauged catchment. The assumption is valid because the catchments share similar geographic, geologic, and landuse characteristics. Analysis of an additional water level gauge downstream supported this presumption. Additionally, specific critical infrastructure such as bridge decks and inflow culvert dimensions were not surveyed or incorporated into the hydrodynamic modelling given the large scale of the study area. Such infrastructure are typically "weakest links" for fluvial discharge as they can restrict or alter flow and contribute to flooding. This omission reduces the accuracy of our model but considering the extreme flood events being modelled and the large geographic area of the watershed these limitations are acceptable. Finally, this study does not consider the potential for increased flooding from wave run-up as the result of wind, nor does it include additional atmospheric forcings such as the effect of ice build-up in the channel and snow melt in isolation of rainfall.

3.3.2. Future Work

The methods developed here to integrate many varied sources of bathymetry data with topographic lidar data were innovative and successful. However, data collection and analysis time would be reduced, and model results improved, if an area were surveyed with topographic-bathymetric lidar, which would inherently provide a high resolution seamless land-sea DEM. We anticipate conducting future flood risk studies that consider the combined effects of fluvial and coastal flooding at NSCC with our recently acquired topographic-bathymetric lidar system, and we expect to build even further on the modelling methodologies developed here using lidar-derived seamless bathymetry-land DEMs.

4. Conclusions

This study modelled combined river discharge and ocean tide-surge hydrodynamics to map flood risk using a combination of innovative GIS tools and methodologies and a sophisticated hydrodynamic model that was established for the study area using a flexible mesh representation of the hydrography and topography.

Discharge was simulated for events that represent a typical annual maximum runoff and extreme events with at least one occurrence within a 50 and 100 year return period based on the EC gauge time-series data measured upstream of Bridgewater. Tide and storm surge events or the equivalent of long term sea-level

rise were simulated by using the predicted maximum high tide during 2012 and adding a 2 and 3 m storm surge to the ocean level seaward of the mouth of the river. In total nine simulations were carried out using a combination of three discharge levels coupled with three tidal-surge levels. For extreme events that are dynamic in nature, the maximum water level can occur at different places and at different times during the simulation. The maximum flood extent for each simulation was examined and the maximum water level for the duration of the simulation was extracted and merged into one file and used in the GIS to map the maximum flood extent and water depth.

Areas upstream of Bridgewater appear most vulnerable to fluvial discharge events and maps demonstrate the areas that are most vulnerable. Areas downstream of Bridgewater appear to be most vulnerable to storm surge and sea-level rise. Infrastructure including roads, buildings and the municipal wastewater (e.g., lift stations) were intersected with the flood layers to map areas at greatest risk. The road information was converted to points every 10 m and analyzed along with the building points and wastewater infrastructure where the flood depth information for each for each of the nine simulations was appended to their respective attribute tables. There are areas where the combined effects of large discharge with elevated sea-levels produce higher water levels than any single event on its own. No adaptation measures have been considered as that was beyond the scope of this current project. However, the information provided from this study will allow the municipality and provincial departments such as the Nova Scotia Department of Transportation and Infrastructure Renewal the ability to evaluate the risk of flooding from large river discharge events and storm surge or longer term sea-level rise and their combined effects and begin considering adaptation measures to mitigate flooding.

Acknowledgments

We thank the Municipality of the District of Lunenburg for funding this study, and the Town of Bridgewater for contributions and for funding the previous study [1].

Author Contributions

T.W. and K.M. conceived and designed the experiments; K.M. performed the experiment; T.W., K.M. and K.C analyzed the data; K.C. and T.W. contributed analysis; K.M., K.C and T.W. wrote the paper.

Conflicts of Interest

The authors declare no conflict of interest.

References

1. Webster, T.; McGuigan, K.; Collins, K.; MacDonald, C. Integrated River and Coastal Hydrodynamic Flood Risk Mapping of the LaHave River Estuary and Town of Bridgewater, Nova Scotia, Canada. *Water* **2014**, *6*, 517–546.
2. Merwade, V.; Cook, A.; Coonrod, J. GIS techniques for creating river terrain models for hydrodynamic modeling and flood inundation mapping. *Environ. Model. Softw.* **2008**, *23*, 1300–1311.

3. Schubert, J.E.; Sanders, B.F.; Smith, M.J.; Wright, N.G. Unstructured mesh generation and landcover-based resistance for hydrodynamic modeling of urban flooding. *Adv. Water Resour.* **2008**, *31*, 1603–1621.
4. Kliem, N.; Nielsen, J.W.; Huess, V. Evaluation of a shallow water unstructured mesh model for the North Sea—Baltic Sea. *Ocean Model.* **2006**, *15*, 124–136.
5. Wang, L.; Zhao, X.; Shen, Y. Coupling hydrodynamic models with GIS for storm surge simulation: Application to the Yangtze Estuary and the Hangzhou Bay, China. *Front. Earth Sci.* **2012**, *6*, 261–275.
6. Ten Hagen, E. Hydrodynamic River Modelling with D-Flow Flexible Mesh: Case Study of the Side Channel at Afferden and Deest. Master's Thesis, University of Twente, Enschede, The Netherlands, 18 September 2014.
7. Gama, M.C.; Popescu, I.; Mynett, A.; Shenyang, L.; van Dam, A. Modelling extreme flood hazard events on the middle Yellow River using DFLOW-flexible mesh approach. *Nat. Hazards Earth Syst. Sci. Discuss.* **2013**, *1*, 6061–6092.
8. Gallegos, H.A.; Schubert, J.E.; Sanders, B.F. Two-dimensional, high-resolution modeling of urban dam-break flooding: A case study of Baldwin Hills, California. *Adv. Water Resour.* **2009**, *32*, 1323–1335.
9. Mtamba, J.; van der Velde, R.; Ndomba, P.; Zoltán, V.; Mtalo, F. Use of Radarsat-2 and Landsat TM Images for Spatial Parameterization of Manning's Roughness Coefficient in Hydraulic Modeling. *Remote Sens.* **2015**, *7*, 836–864.
10. Mason, D.C.; Horritt, M.S.; Bates, P.D.; Hunter, N.M. Improving models of river flood inundation using remote sensing. In *New Developments and Challenges in Remote Sensing*; IOS Press: Amsterdam, The Netherlands, 2007.
11. Cobby, D.M.; Mason, D.C.; Davenport, I.J. Image processing of airborne scanning laser altimetry data for improved river flood modelling. *ISPRS J. Photogramm. Remote Sens.* **2001**, *56*, 121–138.
12. Campana, D.; Marchese, E.; Theule, J.I.; Comiti, F. Channel degradation and restoration of an Alpine river related morphological changes. *Geomorphology* **2014**, 230–241.
13. Kinzel, P.; Legleiter, C.; Nelson, J. Mapping River Bathymetry with a Small Footprint Green LiDAR: Applications and Challenges. *JAWRA J. Am. Water Resour. Assoc.* **2013**, *49*, 183–204.
14. Neily, P.D.; Quigley, E.; Benjamin, L.; Stewart, B.; Duke, T. *Ecological Land Classification for Nova Scotia Volume 1—Mapping Nova Scotia's Terrestrial Ecosystems*; Nova Scotia Department of Natural Resources Renewable Resources Branch: Halifax, Canada, 2003; p. 83.
15. Government of Canada, E.C. Real-Time Hydrometric Data—Environment Canada. Available online: http://www.wateroffice.ec.gc.ca/index_e.html (accessed on 8 November 2013).
16. Brown, L. Flooded LaHave Claims Two Lives. South Shore Now, 2003.
17. Talbot, T. *Environment Canada Storm Surge and Heavy Rainfall Warnings*; Meteorological Service of Canada, Environment Canada: Gatineau, Canada, 2015.
18. CBC News Storm Surge Floods Coastal Nova Scotia. Available online: http://www.cbc.ca/news/canada/nova-scotia/storm-surge-floods-coastal-nova-scotia-1.1300403 (accessed on 7 April 2015).
19. CBC News Nova Scotia Flooded Roads Slowly Reopening. Available online: http://www.cbc.ca/news/canada/nova-scotia/nova-scotia-flooded-roads-slowly-reopening-1.2870854 (accessed on 7 April 2015).

20. Church, J.A.; Gregory, J.M.; Huybrechts, P.; Kuhn, M.; Lambeck, K.; Nhuan, D.; Qin, D.; Woodworth, P.L. Changes in Sea Level. In *Climate Change 2001*: *The Scientific Basis: Contribution of Working Group I to the Third Assessment Report of the Intergovernmental Panel*; Douglas, B.C., Ramirez, A., Eds.; Cambridge University Press: Cambridge, UK, 2001.
21. Meehl, G.A.; Stocker, T.F.; Collins, W.D.; Friedlingstein, P.; Gaye, A.T.; Gregory, J.M.; Kitoh, A.; Knutti, R.; Murphy, J.M.; Noda, A.; *et al*. Global Climate Projections. In *Climate Change 2007: The Physical Science Basis. Contribution of Working Group I to the Fourth Assessment Report of the Intergovernmental Panel on Climate Change*; Solomon, S.; Qin, D., Manning, M., Chen, Z., Marquis, M., Averyt, K.B., Tignor, M., Miller, H.L., Eds.; Cambridge University Press: Cambridge, UK; New York, NY, USA, 2007.
22. IPCC. Summary for Policymakers. In *Climate Change 2013: The Physical Science Basis. Contribution of Working Group I to the Fifth Assessment Report of the Intergovernmental Panel on Climate Change*; Stocker, T.F., Qin, D., Plattner, G.K., Tignor, M., Allen, S.K., Boschung, J., Nauels, A., Xia, Y., Bex, V., Midgley, P.M., Eds.; Cambridge University Press: Cambridge, UK, 2013.
23. Rahmstorf, S. A Semi-Empirical Approach to Projecting Future Sea-Level Rise. *Science* **2007**, *315*, 368–370.
24. Rahmstorf, S.; Cazenave, A.; Church, J.A.; Hansen, J.E.; Keeling, R.F.; Parker, D.E.; Somerville, R.C.J. Recent Climate Observations Compared to Projections. *Science* **2007**, *316*, 709–709.
25. Shaw, J.; Taylor, R.B.; Forbes, D.L.; Ruz, M.H.; Solomon, S. *Sensitivity of the Coasts of Canada to Sea-level Rise*; Natural Resources Canada: Calgary, AL, Canada, 1998; pp. 1–79.
26. Peltier, W.R. Global Glacial Isotasy and the Surface of the Ice-Age Earth: The ICE-5G (VM2) Model and GRACE. *Annu. Rev. Earth Planet. Sci.* **2004**, *32*, 111–149.
27. Forbes, D.L.; Manson, G.K.; Charles, J.; Thompson, K.R.; Taylor, R.B. *Halifax Harbour Extreme Water Levels in the Context of Climate Change: Scenarios for a 100-Year Planning Horizon*; Natural Resources Canada: Calgary, AL, Canada, 2009; p. 22.
28. Richards, W.; Daigle, R. *Scenarios and Guidance for Adaptation to Climate Change and Sea Level Rise—NS and PEI Municipalities*; Atlantic Climate Adaptation Solutions Association: Halifax, Canada, 2011; p. 87.
29. Bruce, J.; Burton, I.; Martin, H.; Mills, B.; Mortsch, L. *Water Sector: Vulnerability and Adaptation to Climate Change*; Final Report; The Government of Canada Climate Change Action Fund: Ottawa, Canada, 2000.
30. Mekis, E.; Hogg, W.D. Rehabilitation and analysis of Canadian daily precipitation time series. *Atmos. Ocean* **1999**, *37*, 53–85.
31. Government of Canada, Natural Resources Canada. Canada in a Changing Climate: Atlantic Canada. Available online: http://www.nrcan.gc.ca/earth-sciences/climate-change/community-adaptation/830 (accessed on 6 November 2013).
32. *Toward a Greener Future: Nova Scotia's Climate Change Action Plan*; Nova Scotia Department of Environment: Halifax, Canada, 2009.
33. Madsen, T.; Willcox, N. *When It Rains*, *It Pours Global Warming and the Increase in Extreme Precipitation from 1948 to 2011*; Environment America Research & Policy Center: Washington, DC, USA, 2012.

34. Singh, D.; Tsiang, M.; Rajaratnam, B.; Diffenbaugh, N.S. Precipitation extremes over the continental United States in a transient, high-resolution, ensemble climate model experiment. *J. Geophys. Res. Atmos.* **2013**, *118*, 7063–7086.
35. Toreti, A.; Naveau, P.; Zampieri, M.; Schindler, A.; Scoccimarro, E.; Xoplaki, E.; Dijkstra, H.A.; Gualdi, S.; Luterbacher, J. Projections of global changes in precipitation extremes from Coupled Model Intercomparison Project Phase 5 models. *Geophys. Res. Lett.* **2013**, *40*, 4887–4892.
36. Whitfield, P.H.; Cannon, A.J. Recent Variations in Climate and Hydrology in Canada. *Can. Water Resour. J.* **2000**, *25*, 19–65.
37. Zhang, X.; Harvey, K.D.; Hogg, W.D.; Yuzyk, T.R. Trends in Canadian streamflow. *Water Resour. Res.* **2001**, *37*, 987–998.
38. Najjar, R.G.; Walker, H.A.; Anderson, P.J.; Barron, E.J.; Bord, R.J.; Gibson, J.R.; Kennedy, V.S.; Knight, C.G.; Megonigal, J.P.; O'Connor, R.E.; *et al*. The potential impacts of climate change on the mid-Atlantic coastal region. *Clim. Res.* **2000**, *14*, 219–233.
39. Intergovernmental Panel on Climate Change Working Group II. *The Regional Impacts of Climate Change: An Assessment of Vulnerability*; Cambridge University Press: Cambridge, UK, 1998.
40. Nova Scotia Department of Fisheries and Aquaculture Lake Inventory Maps. Available online: http://novascotia.ca/fish/programs-and-services/industry-support-services/inland-fisheries/lake-inventory-maps/ (accessed on 16 April 2015).
41. Webster, T.; McGuigan, K.; MacDonald, C. *Lidar Processing and Flood Risk Mapping for Coastal Areas in the District of Lunenburg, Town and District of Yarmouth*, *Amherst*, *County Cumberland*, *Wolfville and Windsor*; Atlantic Climate Adaptation Solutions Association: Halifax, Canada, 2011; p. 130.
42. Pirzadeh, S. Structured background grids for generation of unstructured grids by advancing-front method. *Am. Inst. Aeronaut. Astronaut.* **1993**, *31*, 257–265.
43. DHI MIKE 21 Toolbox. *Global Tide Model—Tidal Prediction*; Aerospace Research Central: Reston, VA, USA, 2014.